Supplemental Material for "Air entrapment of a neutral drop impacting onto a flat solid surface in electric fields"

Yu Tian[1], Yanchu Liu[2], Zihan Peng[1], Chenghao Xu[2], Dong Ye[1], Yin Guan[3], Xinping Zhou[1,4], Weiwei Deng[2]†, and YongAn Huang[1]†

[1]State Key Laboratory of Digital Manufacturing Equipment and Technology, Huazhong University of Science and Technology, Wuhan 430074, China

[2]Department of Mechanics and Aerospace Engineering, Southern University of Science and Technology, Shenzhen 518055, China

[3]School of Energy and Power Engineering, Huazhong University of Science and Technology, Wuhan 430074, China

[4]School of Mechanical Science and Engineering, Huazhong University of Science and Technology, Wuhan 430074, China

(Received xx; revised xx; accepted xx)

In this supplementary material we describe the details of some experimental and numerical results as well as derivation for the scaling law of the critical electric field. In §1, we verified the accuracy of the numerical model and experiments. In §2 we describe the numerical results details. In §3 we give a more detailed description of the derivation for the scaling law of critical electric field.

† Email address for correspondence: yahuang@hust.edu.cn; dengww@sustech.edu.cn

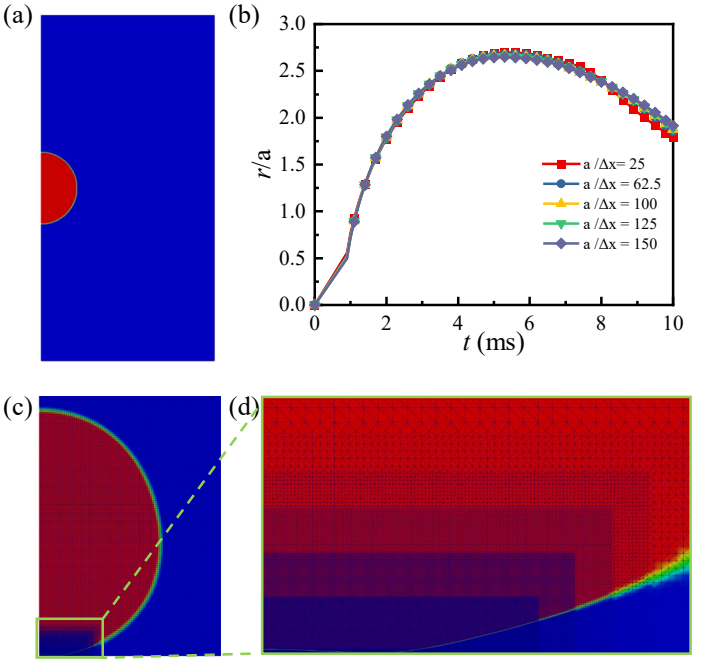

FIGURE S1. (a)The computational domain. (b)The grid independence test. (c-d)Diagram of the local refinement mesh.

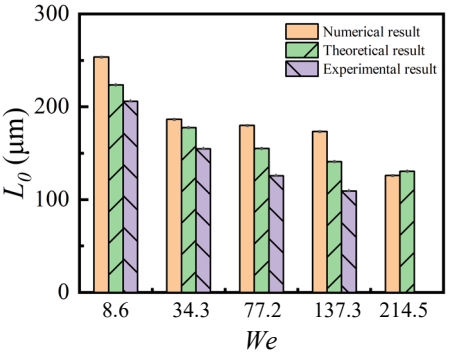

FIGURE S2. Comparison of the initial contact radius (L_0) from numerical, theoretical and experimental results at different velocities, U without electric field.

1. Experimental setup and numerical model

The grid independence test is conducted by comparing the spreading speed of the transient solutions to the max spread radius for different grid resolutions. The drop radius is $1.25mm$, and $We = 34.3$. Five different grid sizes are employed, namely, $a/\triangle x = 25$, $a/\triangle x = 62.5$, $a/\triangle x = 100$, $a/\triangle x = 125$, and $a/\triangle x = 150$, where $\triangle x$ represents the grid spacing in the computational region (figure S1a), and the evolution of the spreading radius with time is plotted in figure S1(b). The difference between the four finer grids is quite small. Here, a grid size of $a/\triangle x = 62.5$ is used to reduce the computational effort, but local encryption is performed at the location of contact with the substrate to capture the evolution of the bottom air film in figure S1(c-b), where $a/\triangle x = 4000$ ($\triangle x = 0.2$ μm).

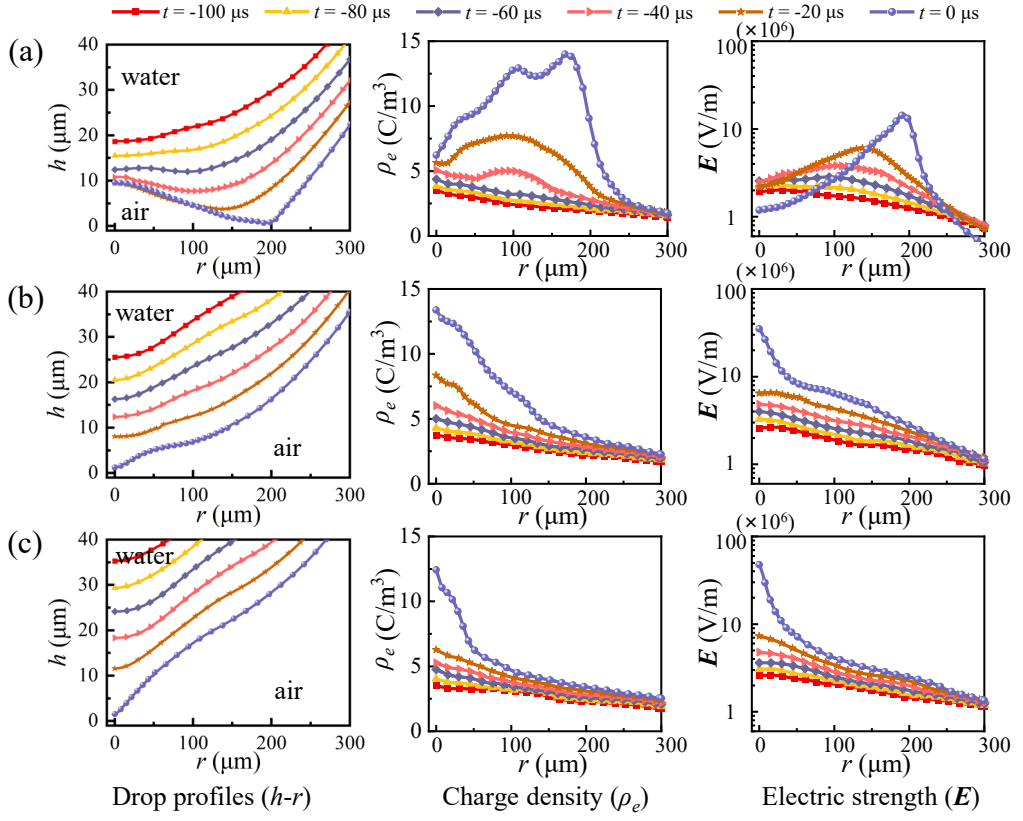

FIGURE S3. Comparison of the charge density (ρ_e) and the electric field strength $\boldsymbol{E}_B$ of the profile on the drop bottom surface in representative contact states before the touchdown. (a) Annular contact mode at $\Gamma_E = 0.17$. (b) Multiple contact mode at $\Gamma_E = 0.26$. (c) Centre contact mode at $\Gamma_E = 0.34$. The time interval is 20 μs.

In figure S2, the comparison of the initial contact radius (L_0) from numerical, theoretical and experimental results at different velocities without electric field shows good agreement and the initial contact radius reduces with the increase of We.

2. Experimental and numerical results

Figure S3 shows the specific data of ρ_e and $\boldsymbol{E}$ of the profile of the drop bottom in the three contact modes. With $\Gamma_E = 0.17$, the charge density near the contact line increases when the bottom of the drop deforms into a dimple. This is owing to the larger curvature at the edge of the air disc, which results in a large electric field there (Figure S3a). With $\Gamma_E = 0.26$, the bottom of the drop sharpens up before $h = 20$ μm. Therefore, the polarized charges accumulate at the lowest of the bottom surface and dramatically increase the electric field (figure S3b). With $\Gamma_E = 0.34$, the charge density at the contact centre is higher and results in a larger electric field (figure S3c).

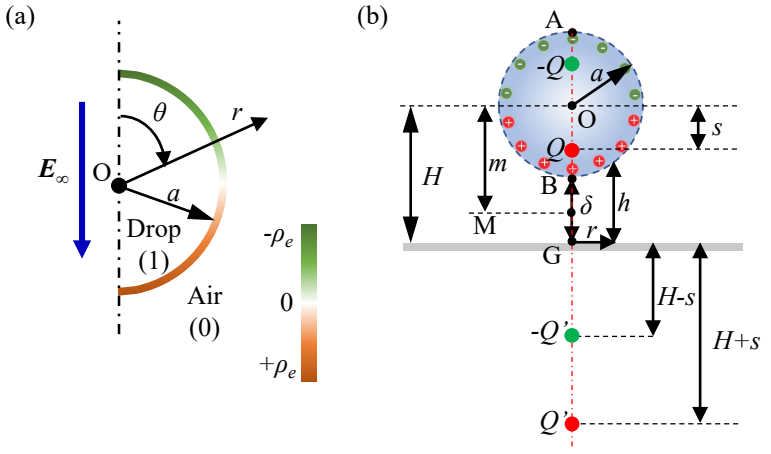

FIGURE S4. (a)Schematic representation of ρ_e distribution in polar coordinates. (b) Schematic diagram of the mirror charge model of the charge dipole simplified by the drop in the electric field when it is close to the grounded substrate.

3. Scaling law of critical electric field

3.1. *The amount of polarized charge (Q) on the drop surface*

The surface charge induced by the electric field reconstructs the space electric field simultaneously, due to the strong coupling between the charge and the electric field. Taylor & G. (1966) gave an analytical solution to the electric field of a suspended drop in an electric field, as shown in figure S4(a). The spatial potential Φ in polar coordinates (r, θ) is

$$\Phi_1 = \frac{3r}{2+R}\boldsymbol{E}_\infty \cos\theta, \tag{3.1}$$

$$\Phi_0 = (r + \frac{1-R}{2+R}\frac{a^3}{r^2})\boldsymbol{E}_\infty \cos\theta, \tag{3.2}$$

where $R = \sigma_1/\sigma_0$ is the electrical conductivity ratio. The electric field along the radius direction (r) is

$$E_{1r} = -\frac{\partial \Phi_1}{\partial r} = -\frac{3}{2+R}\boldsymbol{E}_\infty \cos\theta, \tag{3.3}$$

$$E_{1\theta} = -\frac{\partial \Phi_1}{r\partial\theta,} = \frac{3}{2+R}\boldsymbol{E}_\infty \sin\theta, \tag{3.4}$$

$$\boldsymbol{E}_{0r} = -\frac{\partial \Phi_0}{\partial r} = -\left[1 + \frac{2(R-1)}{2+R}\frac{a^3}{r^3}\right]\boldsymbol{E}_\infty \cos\theta, \tag{3.5}$$

$$E_{0\theta} = -\frac{\partial \Phi_0}{r\partial\theta} = \left[1 - \frac{R-1}{2+R}\frac{a^3}{r^3}\right]\boldsymbol{E}_\infty \sin\theta. \tag{3.6}$$

The electric field strength at the drop surface parallel ($\boldsymbol{E}_P$, $\theta = 0°$) and vertical to ($\boldsymbol{E}_V$, $\theta = 90°$) the direction of the electric field ($\boldsymbol{E}_\infty$) are plotted in figure S5(a), with the parameters (R = 2.5,and a = 1 mm) (Lopez-Herrera *et al.* 2011). It confirms that the electric field in the simulation is consistent with the Taylor's analytical solution.

Based on the Gauss's theorem ($\rho_e = -\varepsilon \boldsymbol{E}_r$), the spatial distribution of charge density

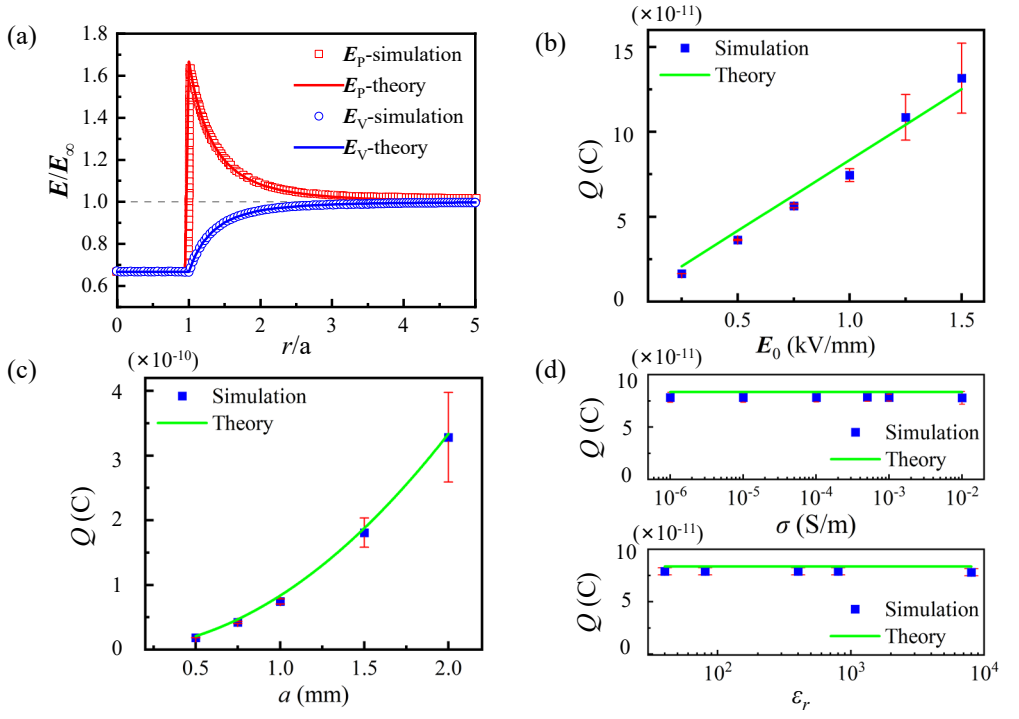

FIGURE S5. (a) Comparison of the simulated and theoretical results for the change of the electric field at the drop surface parallel ($\boldsymbol{E}_P$, $\theta = 0°$) and vertical to ($\boldsymbol{E}_V$, $\theta = 90°$) the direction of the electric field. The electric fields are dimensionless with $\boldsymbol{E}/\boldsymbol{E}_0$ and r/a. (b) The amount of the polarization charge with different electric field strengths. (c) The amount of the polarization charge with different radii of the drop. (d) The amount of the polarization charge with varying conductivity and dielectric value of the drop.

(ρ_e) is

$$\rho_e = -\varepsilon_0 \left(1 + \frac{2\,(R-1)\,a^3}{(2+R)\,r^3}\right) \boldsymbol{E}_\infty \cos(\theta)\,. \tag{3.7}$$

The amount of the electric polarization charge (Q) can be obtained by integrating the ρ_e on the top or bottom hemispherical surface:

$$Q = 2\ \pi \int_0^{\frac{\pi}{2}} \rho_e r^2 \sin(\theta)\ \mathrm{d}\theta = -\frac{\pi\varepsilon_0 \left(2a^3R + r^3R - 2a^3 + 2r^3\right)}{r\,(2+R)} \boldsymbol{E}_\infty. \tag{3.8}$$

Considering the charge only exists at the interface of the drop ($r = a$), the charge amount (Q) at the hemispherical surface is

$$Q = -\frac{3\pi\varepsilon_0 a^2 R}{2+R} \boldsymbol{E}_\infty, \tag{3.9}$$

in which $R \approx 5.5 \times 10^{42}$, so the charge quantity Q can be simplified as

$$Q = -3\pi\varepsilon_0 a^2 \boldsymbol{E}_\infty, \tag{3.10}$$

where the negative sign ("$-$") means that the electrical properties of the polarized charge (Q) is opposite to $\boldsymbol{E}_\infty$. The polarized charge obtained numerically $(Q_{Simulation})$ agree with the theory (Q_{Theory}) very well, as shown in figure S5(b-d), qualitatively supporting

the notion that the surface polarized charge of the drop is unchanged when the drop approaches the substrate.

3.2. *Mirror charge model of the charge dipole*

The separation of polarized surface charge allows us to treat the drop as a charge dipole. We further use the mirror charge model of this dipole to quantify explain the rapid growth of the $\boldsymbol{E}_B$ and $\boldsymbol{f}_{esB}$ at the bottom of the drop. As shown in figure S4 (b), we assume: i) The deformation of the drop is small and the drop can be treated as a sphere for the purpose of mirror charge quantification; ii) The charge is distributed equally on the top and bottom of the drop hemisphere; iii) The internal electric field of the drop is negligible; iv) The substrate is a conductive plane of zero potential. The axial symmetry suggests that the electric field of the non-uniformly distributed induced charges is equivalent to that generated by point charges that located on the central axis of the drop. We assume the distance from the centre of the drop (point O) to the point charge is s. Here H is the distance between O and the substrate (point G). According to the method of mirror charge (Papadopoulos 1963), there is a point charge with opposite charges at a symmetrical position on the lower side of the grounded conductive substrate. The space electric field formed by the surface charge can be replaced by four equivalent point charges. First, the potential at point A on the upper of the drop is

$$\Phi_{\mathrm{A}} = \frac{1}{4\pi\varepsilon_0}\left(\frac{-Q}{a-s} + \frac{Q}{a+s} + \frac{-Q^{'}}{2H+a-s} + \frac{Q^{'}}{2H+a+s}\right). \tag{3.11}$$

The electric potential at point B at the lower part of the drop is

$$\Phi_B = \frac{1}{4\pi\varepsilon_0}\left(\frac{-Q}{a+s} + \frac{Q}{a-s} + \frac{-Q^{'}}{2H-a-s} + \frac{Q^{'}}{2H-a+s}\right). \tag{3.12}$$

Because the electric field intensity inside the drop is approximately 0:

$$\boldsymbol{E}_1 = -\frac{3}{2+R} \approx 0. \tag{3.13}$$

It can be considered that:

$$\Phi_A = \Phi_B. \tag{3.14}$$

According to the mirror charge model, it is first assumed that the induced mirror charge $Q' = Q$. Combining the above equations, the location of charge centre (s) can be expressed as:

$$s = \sqrt{a^2 - 2aH + 4H^2 - 2\sqrt{5a^2H^2 - 4rH^3}}. \tag{3.15}$$

The distance between the drop and the substrate is $\delta = H - a$. Substituting that into equation (3.15), the location of charge centre (s) is

$$s = \sqrt{a^2 - 2\ a\ H + 4\ H^2 - 2\sqrt{5a^2(a+\delta)^2 - 4r(a+\delta)^3}}. \tag{3.16}$$

Expanding and simplifying the above equation yields:

$$s = \sqrt{-a^2 - 2a\delta - 2aH + 4H^2}. \tag{3.17}$$

Equation (3.17) that s approaches a with the decrease of δ, which means the charge on the surface of the drop is concentrated at point B when the drop contacts the substrate. The electric potential Φ_D for any point M between the bottom of the drop (B) and the

substrate (G) is

$$\Phi_{\mathrm{M}} = \frac{Q}{4\pi\varepsilon_0}\left(\frac{-1}{m+a}+\frac{1}{m-a}+\frac{-1}{2H-m-a}+\frac{1}{2H-m+a}\right). \tag{3.18}$$

The electric field at any point M is

$$\Phi_{\mathrm{M}}{}'(m) = \frac{Q}{4\pi\varepsilon_0}\left(\frac{1}{(m+s)^2}+\frac{-1}{(m-s)^2}+\frac{-1}{(2H-m-s)^2}+\frac{1}{(2H-m+s)^2}\right). \tag{3.19}$$

The electric field at point B ($m = a$) is

$$\boldsymbol{E}_B = \frac{Q}{4\pi\varepsilon_0}\left(\frac{1}{(a+s)^2}-\frac{1}{(a-s)^2}-\frac{1}{(2H-a-s)^2}+\frac{1}{(2H-a+s)^2}\right). \tag{3.20}$$

Substituting $H = \delta + a$ into the above equation:

$$\boldsymbol{E}_B = \frac{Q}{4\pi\varepsilon_0}\left(-\frac{8s\,(a+\delta)\left(a^4+4a^3\delta-2a^2s^2+8a^2\delta^2-4a\delta s^2+8r\delta^3+s^4\right)}{(a+s)^2(a-s)^2(a+2\delta-s)^2(a+2\delta+s)^2}\right). \tag{3.21}$$

Expanding and omitting the second order minima yields

$$\boldsymbol{E}_B = \frac{Q}{4\pi\varepsilon_0}\left(\frac{-8a^5s-40a^4s\delta+16\ a^3s^3+48\ a^2s^3\delta-8\ a\ s^5-8s^5\delta}{a^8-4a^6s^2+6\ a^4s^4-4\ a^2s^6+s^8}\right), \tag{3.22}$$

which can be simplified as

$$\boldsymbol{E}_B = \frac{Q}{4\pi\varepsilon_0}\left(-\frac{8\left((-a-\delta)\,s^2+r^2\,(a+5\delta)\right)s}{(a-s)^3(a+s)^3}\right). \tag{3.23}$$

After substituting (3.17)

$$\boldsymbol{E}_B = \frac{Q}{4\pi\varepsilon_0}\left(-\frac{(2a+\delta)\,(a+2h)}{2\delta(a+\delta)^3}\right). \tag{3.24}$$

By omitting the first-order fractional quantities for simplification and substituting (3.10), the electric field at the bottom of the drop can be obtained as

$$\boldsymbol{E}_B = \frac{Q}{4\pi\varepsilon_0}\left(\frac{-1}{a\delta}\right) = \frac{3a}{4\delta}\boldsymbol{E}_\infty. \tag{3.25}$$

Equation (3.25) suggests that the $\boldsymbol{E}_B$ at the bottom of the drop increases sharply as δ decreases. The characteristic electric field stress $\boldsymbol{f}_{esB}$ is

$$\boldsymbol{f}_{\mathrm{esB}} = \frac{1}{2}\varepsilon_0{\boldsymbol{E}_B}^2 = \frac{9\varepsilon_0a^2}{32\delta^2}\boldsymbol{E}_\infty^2. \tag{3.26}$$

Therefore, the scaling laws of $\boldsymbol{E}_B$ and $\boldsymbol{f}_{esB}$ versus δ are

$$\boldsymbol{E}_B \sim \frac{a}{\delta}\boldsymbol{E}_\infty;\ \boldsymbol{f}_{\mathrm{esB}} \sim \frac{\varepsilon_0a^2}{\delta^2}\boldsymbol{E}_\infty^2. \tag{3.27}$$

The numerical results of E_B and $\boldsymbol{f}_{esB}$ with different δ are shown in figure S6. $\boldsymbol{E}_B$ and $\boldsymbol{f}_{esB}$ increase exponentially when $\delta < 1mm$. When $\Gamma_E < 0.26$, the annular contact with reduced air disc appears. The charge accumulates in the ring around the air disc and fails to concentrate to one point, resulting in slopes smooth than -1 (for $\boldsymbol{E}_B$) and -2 (for $\boldsymbol{f}_{esB}$) in the logarithm scale in figure S6 respectively. When $0.26 < \Gamma_E < 0.68$, the point

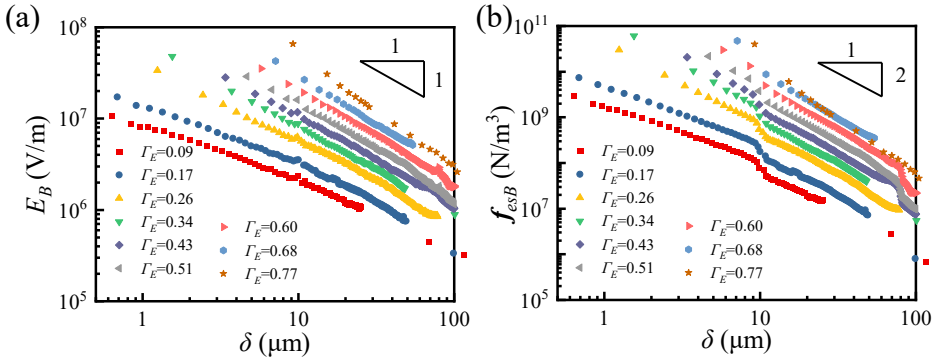

FIGURE S6. The $\boldsymbol{E}_B \sim c_1/\delta$ and $\boldsymbol{f}_{esB} \sim c_2/\delta^2$ formula is used to fit the $\boldsymbol{E}_B$ (a) and $\boldsymbol{f}_{esB}$ (b) data at the lowest point of the drop extracted from the simulation.

contact states occur, and the charge can accumulate at the bottom apex of the drop. In this range of electric feild, the slopes are approximately -1 (for $\boldsymbol{E}_B$) and -2 (for $\boldsymbol{f}_{esB}$) in the logarithm scale in figure S6. When $\Gamma_E > 0.68$, the ellipsoid deformation of the drop is significant, which deviates further from the spherical drop assumption, resulting in slopes steeper than -1 (for $\boldsymbol{E}_B$) and -2 (for $\boldsymbol{f}_{esB}$) in the logarithm scale in figure S6.

3.3. *Calculation of the Lubrication pressure p_g*

Klaseboer *et al.* (2014) shown that for the charge neutral drop impact, the profile of the drop bottom surface is governed by the balance between drop inertia and lubrication pressure. While exposed in an electric field, the additional electric stress may become comparable to the lubrication pressure. The gas film is mainly affected by the combined effects of gravity, Laplace pressure ($p_{laplace} = 2\gamma/a$), the lubrication pressure (p_g) and the electric stress ($\boldsymbol{f}_{esB}$). Here gravity and surface tension are relatively small and can be neglected.

The airflow is assumed to be incompressible because p_g is much smaller than the ambient pressure ($P_0 = 10^5 Pa$) in this study, which also can be reflected by the compressibility factor $\epsilon \equiv P_0/\left(a\mu_0^{-1}\boldsymbol{U}^7\rho_1^4\right)^{1/3}$ is bigger than 1/3 (Mandre *et al.* 2009; Li & Thoroddsen 2015). When a drop impacts a flat and smooth surface without electric field, the air film between the drop and the substrate can be regarded as a lubricating film with a uniform thickness. The lubrication pressure distribution at the bottom of the drop can be obtained by the lubrication approximation of the Reynolds equation in axisymmetric form Chan *et al.* (2011):

$$\frac{\partial}{\partial x}\left(\frac{\rho_0 h^3}{12\mu_0}\frac{\partial p}{\partial x}\right) + \frac{\partial}{\partial y}\left(\frac{\rho_0 h^3}{12\mu_0}\frac{\partial p}{\partial y}\right) = \frac{\partial\left(\rho_0 h\right)}{\partial t}, \tag{3.28}$$

where h is the distance from the substrate to the sphere (that is thickness of air film), ρ_0 is the density of air, μ_0 is the dynamic viscosity of air and p is the air pressure (that is lubrication pressure). The last term in the (3.28) represents the time dependent portion of the Reynolds equation.

It is reasonable to assume the gas is incompressible in this experimental conditions. Hence, the ρ_0 does not change. Meanwhile, the whole model is axisymmetric, the second term on the left of (3.28) can be ignored. The lubrication pressure distribution at the bottom of the drop can be obtained by lubrication approximation of the Reynolds

equation in axisymmetric form (Chan *et al.* 2011):

$$\frac{1}{r}\frac{\partial}{\partial r}\left(\frac{h^3}{12\mu_0}r\frac{\partial p}{\partial r}\right)=\frac{\partial\left(h\right)}{\partial t}. \tag{3.29}$$

Integrating r on both sides of the equal sign simultaneously:

$$\frac{h^3}{12\mu_0}\mathrm{r}\,\frac{\partial p}{\partial r}=\frac{\partial h}{2\partial t}\mathrm{r}^2, \tag{3.30}$$

Further the above equation can be expressed as

$$\frac{\partial p}{\partial r}=\frac{6\mu_0\,\mathrm{r}}{h^3}\frac{\partial h}{\partial t}. \tag{3.31}$$

After substituting $\boldsymbol{U}=-\partial h\left(r,t\right)/\partial t$ into it, we obtain

$$\frac{\partial p}{\partial r}=-\frac{6\mu_0\,\mathrm{r}}{h^3}\boldsymbol{U}. \tag{3.32}$$

By changing the differential elementary, the above equation can be expressed as

$$\frac{\partial p}{\partial r^2}=-\frac{3\mu_0}{h^3}\boldsymbol{U}. \tag{3.33}$$

Here h is a function of r:

$$h=\delta+a-\sqrt{a^2-r^2},(0\leqslant r\leqslant a). \tag{3.34}$$

The above equation can be found as

$$r^2=-2\delta a+2ha-\delta^2+2h\delta-h^2. \tag{3.35}$$

The above equations are differentiated for h:

$$\frac{\partial r^2}{\partial h}=2a+2\delta-2h. \tag{3.36}$$

Solving equations (3.33), (3.36) jointly, we can obtain

$$p_g=\frac{\partial p}{\partial r^2}\frac{\partial r^2}{\partial h}=-6\mu_0(\frac{a+\delta}{h^3}-\frac{1}{h^2})\boldsymbol{U} \tag{3.37}$$

Integrating the above equations on h:

$$p_g=-6\mu_0(-\frac{a+\delta}{2h^2}+\frac{1}{h})\boldsymbol{U}+C, \tag{3.38}$$

where C is the constant pressure in the continuous phase (p_0) in $r\geqslant a$. Substitute equation (3.34) into the above equation

$$p_g=-3\mu_0\frac{\delta+a-2\sqrt{a^2-r^2}}{\left(\delta+a-\sqrt{a^2-r^2}\right)^2}\boldsymbol{U}+C. \tag{3.39}$$

Here the atmospheric pressure is used as the reference zero point, $p_{(r=a)}=0$ Pa, resulting in that C can be solved as $C=3\mu_0\boldsymbol{U}/a$. The lubrication pressure can be further expressed as

$$p_g=-3\mu_0\frac{\delta+a-2\sqrt{a^2-r^2}}{\left(\delta+a-\sqrt{a^2-r^2}\right)^2}\boldsymbol{U}+\frac{3\mu_0}{a}\boldsymbol{U}. \tag{3.40}$$

At the position of the drop vertical axis ($r=0$), the lubrication pressure (p_g) can be

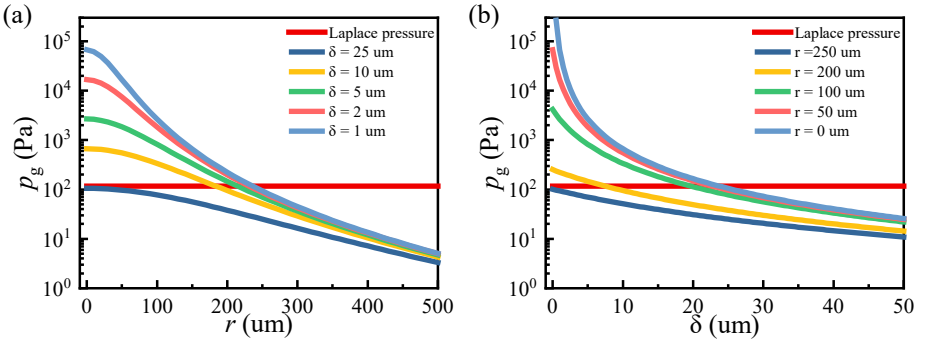

FIGURE S7. (a)The distribution of lubrication pressure (p_g) along the radius r. (b) The distribution of lubrication pressure (p_g) along the distance δ.

simplified as

$$p_g = \frac{3\mu_0 a}{\delta^2} \boldsymbol{U}. \tag{3.41}$$

Here the radius of the drop is $a = 1.25$ mm and the impact velocity is $U = 1$ m/s. In this case, the Laplace pressure of the drop is $p_{Laplace} = 2\gamma/a = 116.32$ Pa. Figure S7 shows the distribution of lubrication pressure (p_g) when the drop is close to the substrate. As the drop approaches the substrate, the lubrication pressure begins to increase and exceeds the surface tension within a certain range, causing the bottom of the drop to deform into a dimple. The highest pressure point is always generated at the symmetry axis and decays rapidly along the radius direction, which is the key factor of the initial contact diameter. The lubrication pressure becomes negligible beyond the radius of 250 microns, as shown in figure S7(a). The lubrication pressure increases sharply when $\delta < 25$ μm, as shown in figure S7(b).

REFERENCES

CHAN, DEREK Y. C., KLASEBOER, EVERT & MANICA, ROGERIO 2011 Film drainage and coalescence between deformable drops and bubbles. *Soft Matter* **7** (6), 2235–2264.

KLASEBOER, E., MANICA, R. & CHAN, D. Y. 2014 Universal behavior of the initial stage of drop impact. *Phys Rev Lett* **113** (19), 194501.

LI, E. Q. & THORODDSEN, S. T. 2015 Time-resolved imaging of a compressible air disc under a drop impacting on a solid surface. *J. Fluid Mech.* **780**, 636–648.

LOPEZ-HERRERA, J. M., POPINET, S. & HERRADA, M. A. 2011 A charge-conservative approach for simulating electrohydrodynamic two-phase flows using volume-of-fluid. *Journal of Computational Physics* **230** (5), 1939–1955.

MANDRE, S., MANI, M. & BRENNER, M. P. 2009 Precursors to splashing of liquid droplets on a solid surface. *Phys Rev Lett* **102** (13), 134502.

PAPADOPOULOS, M 1963 Classical electrodynamics (jd jackson). *SIAM Review* **5** (1), 82.

TAYLOR & G. 1966 Studies in electrohydrodynamics. i. the circulation produced in a drop by electrical field. *Proceedings of the Royal Society A Mathematical Physical* **291** (1425), 159–166.